



Basement configuration and structural mapping using aeromagnetic data analysis of El Galala El Qibliya plateau area, Northeastern Desert, Egypt

Wael Dosoky¹ · Sayed O. Elkhateeb¹ · Mohamed Aboalhassan¹

Received: 20 September 2022 / Accepted: 6 November 2022 / Published online: 25 November 2022
© The Author(s), under exclusive licence to Springer Nature Switzerland AG 2022

Abstract

Aeromagnetic data at El Galala El Qibliya Plateau area were processed and analysed to determine the basement depth and the structural trends that provided an understanding of the geological background for exploring hydrocarbons and mineral resources in the area. The magnetic data were interpreted qualitatively and quantitatively. Edge detection techniques (EDT) such as the analytic signal (AS), horizontal gradient magnitude (HGM), tilt derivative (TDR), centre for exploration targeting method (CET), and Euler deconvolution (ED) were used to locate the lineament structures within the investigated area. The depth of the magnetic sources was estimated using analytical signal (AS), source parameter imaging (SPI), and 2D modeling. The results show that the southeastern and the northeastern parts of the area are highly affected by lineament structures that might be related to faults/contacts which are mainly controlled by the NW–SE, NNW–SSE, and NE–SW trends. The AS depth result ranges from 225 to 3387 m while the SPI depth results range from 280 to 3703 m. more clear picture of the basement topography surface was obtained by the generation of two 2D models across the area. The obtained models show that the basement surface exhibits a depth varying from 50 to 3500 m with a horst and graben morphology of the basement surface. The overall results reveal that the study area is considered a promising area for mineral exploration and hydrocarbon resources, and further investigation studies should be considered for such a promising area.

Keywords El Galala El Qibliya · Aeromagnetic · Basement depth · Lineament structures

Introduction

Among the different geophysical tools, the magnetic method is the oldest and the most widely used for investigating the earth's interior. It is a quick, cheap, and easy tool to be employed in a wide range of subsurface exploration problems from very near surface to locate metalliferous man-made objects, through regional geological mapping to determine large-scale structure, such as in hydrocarbon exploration (Reynolds 2011; Hinze et al. 2013). The magnetic method investigates the earth's subsurface based on the Earth's magnetic field variations that result from the magnetic properties variation of the underlying rocks. In general, igneous and metamorphic rocks have greater magnetic

minerals than sedimentary rocks. This facilitates the determination of basement depth, sedimentary thickness, and mapping of structures (Al-Saud 2014; Anyadiegwu et al. 2017). The aeromagnetic survey is one of the most economical methods in undertaking a geophysical reconnaissance exploration which is used as an initial investigating phase of any regional scale area (Pohl 2011; Dentith and Mudge 2014). It can be used in a wide range of applications, including geothermal, hydrocarbon, groundwater investigation, structural mapping, and mineralogical studies (Tsokas and Papazachos 1992).

The magnetic method has been used for a broad range of applications such as mapping dykes (Hamath et al. 2020), hydrocarbon exploration (Azab 2020), mapping mineral deposits (Osinowo et al. 2020), geothermal investigation (Ramotoroko et al. 2021), imaging sedimentary basins (Nathan et al. 2020), basement depth estimation (Erbek 2021), mapping structure features (Oguama et al. 2021), and Basement architecture determination (Okoro et al. 2022). Many researchers used the magnetic method to determine

✉ Wael Dosoky
wael.desoky@sci.svu.edu.eg

¹ Geology Department, Faculty of Science, South Valley University, Qena, Egypt

basement depths, faults, minerals exploration, and hydrocarbon studies in different areas in Egypt (Ibraheem et al. 2018; Ghazala et al. 2018; Mohamed and Zaher 2020; Araffa et al. 2020; Eweis et al. 2022).

The present work aims to investigate El Galala El Qibliya Plateau area (The southern Galala) using the available aeromagnetic data. The study area is located in the Northeastern Desert of Egypt between Long $32^{\circ} 04' 25''$ & $32^{\circ} 41' 30''$ and Lat $28^{\circ} 27' 21''$ & $28^{\circ} 49' 22''$ to the west of the Gulf of Suez, covering a surface area of about 2400 km^2 (Fig. 1a). It forms a remarkable topographic feature rising to 1460 m above the mean sea level, and the height decrease gradually to the west direction (Fig. 1b). The area under investigation was chosen to carry out this study due to its discriminative geological setting and vital location near the Gulf of Suez, which is considered one of the remarkable sites of hydrocarbon production in Egypt.

Previously, many authors have carried out studies at EL Galala El Qibliya Plateau, mostly involving stratigraphy, petrology, and palaeontology studies (Kuss 1986; Kuss and Leppig 1989; Keheila 2000; Kuss et al. 2000; Ismail and Boukhry 2001; Scheibner et al. 2001). On the other hand, few geophysical studies were performed in the north of the study area at EL Galala El Baharia Plateau e.g. El-Sadek (2009), Saada (2016), Abdelazeem et al. (2019), and Mekkawi et al. (2022) but no sufficient information about the subsurface geology beneath the El Galala El Qibliya Plateau area is available. Accordingly, this work is devoted to interpreting and analysing the aeromagnetic data as a reconnaissance

step for the evaluation of the natural resources, basement depth determination, and structural trends mapping in the El Galala El Qibliya Plateau area.

Geological setting of the study area

The study area exhibits exposed rock units which vary in their origin and ages. The rock types can be distinguished into two main associations: a Precambrian basement complex and Late Palaeozoic to Quaternary sedimentary rocks (Fig. 2). The crystalline rocks are represented by older granite, younger granite, and Dokhan volcanics related to the age of Precambrian as well as more recent Tertiary intrusions of a basaltic dike exists at the central north part of the study area. Regarding the sedimentary rock units association, most of them belong to Cretaceous–Quaternary deposits, except for the central part of the area which is covered by the Araba Formation (Fm) n (Fm) (Lower Cambrian) and Samer El Qa Fm (Lower Carboniferous). The Cretaceous sediments cover the central and the northeastern part and are incorporated in Malha Fm, Wadi Qena Fm, Undifferentiated upper cretaceous deposits, Galala Fm, Umm Omeiyid Fm, Hawashiya Fm, Rakhaiyat Fm, and Sudr Fm. (Conoco Inc 1987, 1989).

The structure patterns of the Gulf of Suez region included within the study area were elucidated by several authors. Moustafa and Khalil (1995) concluded that the Gulf of Suez area was influenced by two main structural phases. The first phase is the late Cretaceous deformation phase

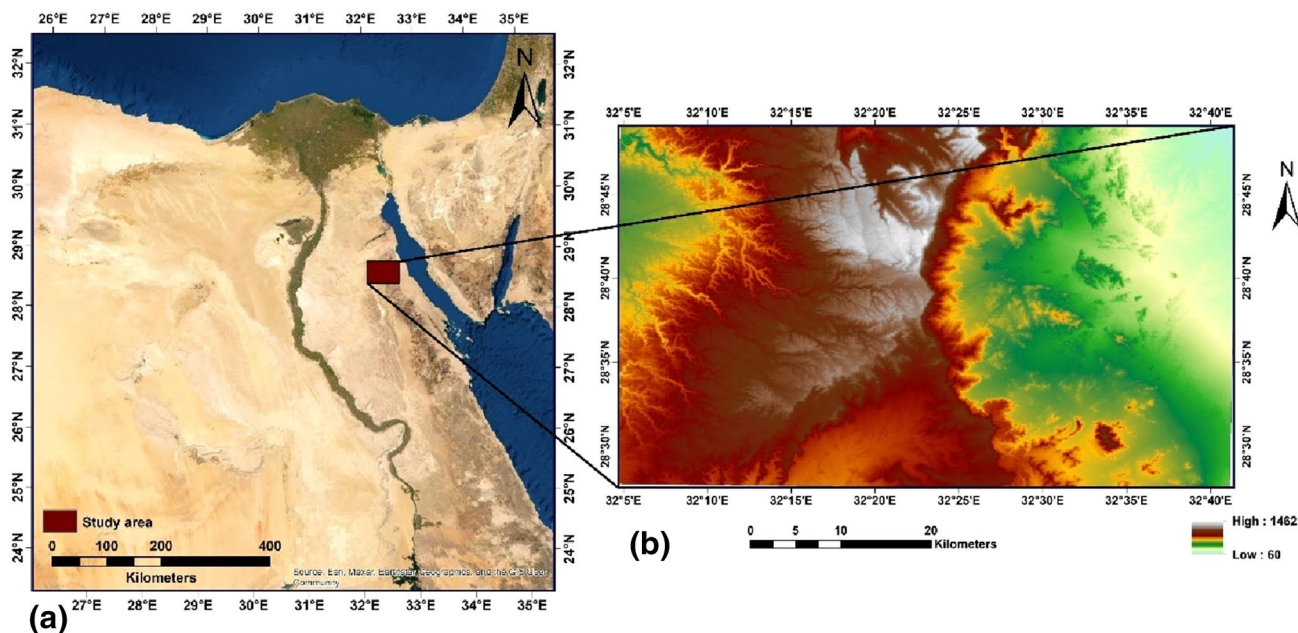
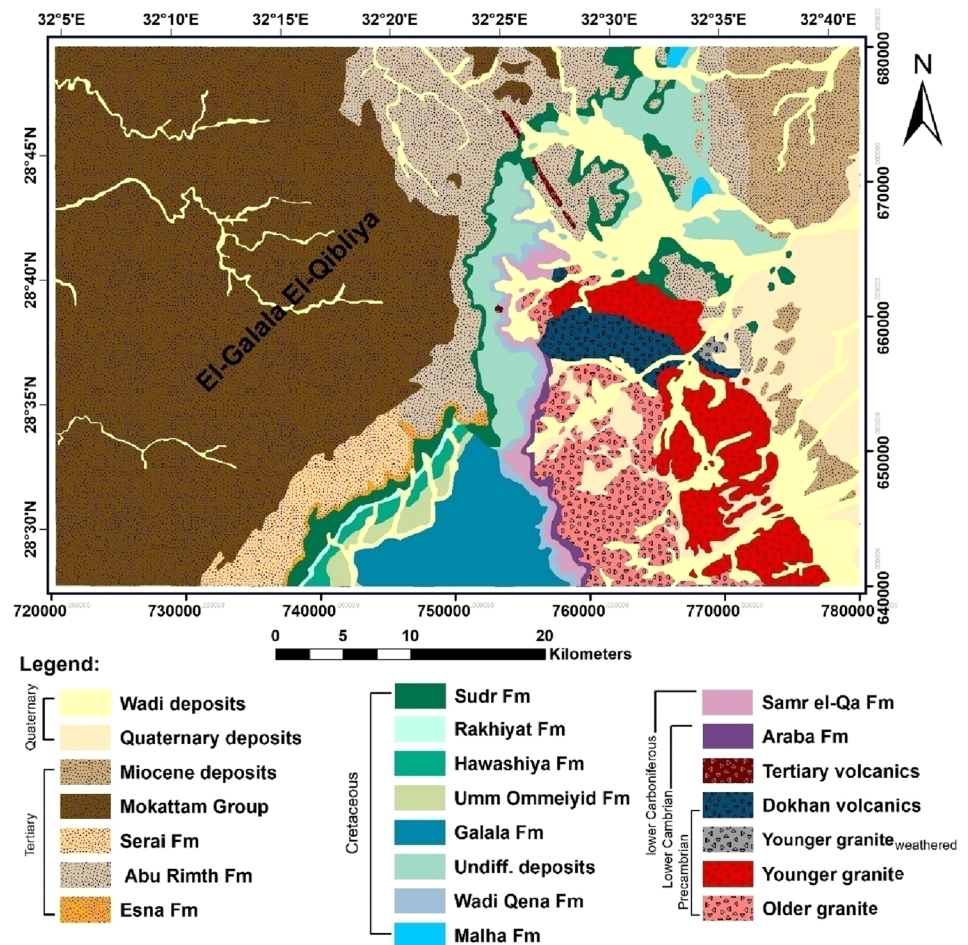


Fig. 1 HYPERLINK "sps:id::fig1|locator::gr1|MediaObject::0" (a) Location map of El Galala El Qibliya plateau area, and (b) a digital elevation model for illustration of its topography and morphology

Fig. 2 Geological map of El Galala El Qibliya plateau area (modified after Conoco 1987)



with NE-SW orientation which was formed as a result of Africa and Eurasia convergence and the Neotethes closure. The second phase was formed during the early Miocene due to the opening of the Suez Rift consequently, deformations of NW-oriented normal faults were formed. In agreement with the above-mentioned conclusions, Younes and McClay (2002) concluded that the structural architecture of the Gulf region is controlled by a complex pattern of faulting with two main trends: NW (Gulf of Suez trend) and NE (Gulf of Aqaba trend). Abdel-Gawad (1970) concluded that there are three main fault systems with N, NW, and WNW that appear to control the structure of the Gulf and Red Sea area.

Methodology

The aeromagnetic data of the investigated area was obtained by digitising the total intensity magnetic map (TIM) with a scale of 1:50,000 after the survey conducted by Aero Service Division, Western Geophysical Company of America in 1984, for the Egyptian General Petroleum Corporation (EGPC) and the Egyptian Geological Survey and Mining

Authority (EGSMA). The survey was executed with a spacing of 1.5 km of flight line oriented in the NE–SW direction (45°/225°) and 10 km tie intervals in the NW–SE direction (135°/315°). Measurements were made at (92.65 m) intervals with an altitude of 120 m of terrain clearance. The total field of the area has an intensity of 42,425 nT, while the mean inclination and declination angle of the ambient field is 39.5 N and 2.1 E, respectively (Aero service 1984).

The (TIM) data were reduced to the pole (RTP) according to Baranov and Naudy (1964) to ameliorate the effect of oblique magnetization. This process followed by the analysis of the power spectrum curve of RTP magnetic data to separate the regional and residual magnetic anomalies. The power spectrum curve (Fig. 4) shows two different linear segments with different frequency bands related to the deep and shallow magnetic sources. The deep-seated magnetic component frequency bands ranging from 0.0 to 0.08 cycles/km, while the shallow magnetic component frequency bands range from 0.08 to 0.35 cycles/km. These bands of frequency were used through the band-pass filter technique to produce the regional and residual component magnetic maps. The analyses of magnetic data in this study

were achieved through qualitative and quantitative interpretation processes. The data were qualitatively interpreted with the aim of delineating the lineaments and their trends using Edge detection techniques (EDT). Various EDT were employed in this study, including the horizontal gradient magnitude (HGM), analytic signal (AS), Euler deconvolution (ED), CET grid analysis, and the tilt angle derivative (TDR). Several authors used EDT for mapping subsurface structural features e.g. (Oguama et al. 2021; Basantaray and Mandal 2022). The quantitative interpretation was achieved by application of several magnetic depth estimation methods such as analysis of power spectrum (Spector and Grant 1970), Source parameters imaging (SPI) (Thurston and Smith 1997), Analytic signal (AS) (Nabighian 1972), Euler deconvolution (ED) (Thompson 1982; Reid et al. 1990), 2D magnetic modelling (Talwani et al. 1959; Talwani and Heirtzler 1964). All processing and enhancement techniques were applied on the RTP magnetic data using the oasis montaj package version 8.4 (Geosoft 2015).

The HGM filter (Cordell and Grauch 1985) is an enhancement technique designed to look at fault and contact features, it usually produces a more exact location for faults. Maxima in the enhanced map indicates source edges. If f is the magnetic field, then the (HGM) is given by:

$$\text{HGM}(x, y) = \sqrt{\left(\frac{\partial f}{\partial x}\right)^2 + \left(\frac{\partial f}{\partial y}\right)^2}, \quad (1)$$

where $\frac{\partial f}{\partial x}$ is the horizontal derivative in the x direction and $\frac{\partial f}{\partial y}$ is the horizontal derivative in the y direction. The usefulness of the HGM technique is it less affected by the noise in the original data and depends on the two horizontal derivatives of the magnetic field (Phillips 2002).

The AS technique is a popular gradient enhancement which is related to magnetic fields by the derivatives. Roest et al. (1992) showed that the amplitude of the AS can be derived from the three orthogonal gradients of the total magnetic field using the expression:

$$|\text{AS}(X, Y, Z)| = \sqrt{\left(\frac{\partial f}{\partial x}\right)^2 + \left(\frac{\partial f}{\partial y}\right)^2 + \left(\frac{\partial f}{\partial z}\right)^2}, \quad (2)$$

where AS (x, y, z) is the amplitude of the analytical signal at x , y , and z directions and f is the observed magnetic anomaly at (x, y) . The AS displays maxima over the source body edges even when the direction of the magnetization is not vertical. The depth of magnetic source bodies can be estimated by the AS techniques from the ratio of the total magnetic analytic signal (AS) Eqs. (2) to the vertical derivative analytic signal (AS1) as given below:

$$\text{AS1} = \sqrt{\left(\frac{\partial f_v}{\partial x}\right)^2 + \left(\frac{\partial f_v}{\partial y}\right)^2 + \left(\frac{\partial f_v}{\partial z}\right)^2} \quad (3)$$

$$D = (\text{AS}/\text{AS1}) * N, \quad (4)$$

where $\frac{\partial f}{\partial x}$, $\frac{\partial f}{\partial y}$, and $\frac{\partial f}{\partial z}$ are the first derivatives in x , y , and z directions of the total magnetic field, f_v is the first vertical derivative of the total magnetic field, D is the depth to the magnetic body, and N is known as a structural index and is related to the geometry of the magnetic source. For example, $N=4$ for sphere, $N=3$ for pipe, $N=2$ for thin dike and $N=1$ for magnetic contact (Nabighian 1972).

The ED technique provides automatic estimates of source location and depth. Therefore, this technique is a boundary locator and depth estimation method (Thompson 1982; Reid et al. 1990). ED is based on solving Euler's homogeneity equation:

$$(x - x^0) \frac{\partial f}{\partial x} + (y - y^0) \frac{\partial f}{\partial y} + (z - z^0) \frac{\partial f}{\partial z} = N(B - f), \quad (5)$$

where B is the regional value of the total magnetic field and (x_0, y_0, z_0) is the position of the magnetic source, which produces the total magnetic field f measured at (x, y, z) and N is called the structural index, which represents the geometry of the magnetic sources e.g. contact ($N=0$), fault ($N=0.5$), sill or dyke ($N=1$), vertical or horizontal cylinder ($N=2$) and sphere ($N=3$). Both Thompson (1982) and Reid et al. (1990) suggested that a correct N value gives the tightest clustering of the Euler solutions around the geologic structure of interest.

The centre for exploration targeting (CET) grid is an effective technique used in the extraction of linear discontinuities and recognition of edges within gravity and magnetic field data. The CET grid technique analyses images texture to detect lineaments along with contacts, boundaries, and edges by subsequent steps that start with the computation of the standard deviation which estimates magnetic variations, phase symmetry to detect ridges, amplitude threshold to detect line segments of the ridges, and skeletonization (line thinning) to generate axial lines (Holden et al. 2012). The CET grid analyses technique was applied to the RTP grid data and the extracted lineaments were measured clockwise from the North automated using the Arc Gis program. These lineament segments were statistically analysed and plotted in the form of rose diagrams using Rockworks software version 17 (rockworks 2018).

The (TDR) filter is defined by Miller and Singh (1994) as the ratio of the first vertical derivative (VDR) to the amplitude of the total horizontal derivative (THDR):

$$\text{TDR} = \tan^{-1}\left(\frac{\text{VDR}}{\text{THDR}}\right), \tag{6}$$

where:

$$\text{VDR} = \left(\frac{\partial f}{\partial z}\right) \tag{7}$$

and

$$\text{THDR} = \sqrt{\left(\frac{\partial f}{\partial x}\right)^2 + \left(\frac{\partial f}{\partial y}\right)^2}. \tag{8}$$

The derivatives $\frac{\partial f}{\partial x}$, $\frac{\partial f}{\partial y}$, and $\frac{\partial f}{\partial z}$ in Eqs. (7) and (8) refer to the first derivatives of the magnetic field (f) in the x , y , and z directions, respectively. The TDR filter is a particularly good edge-detection filter, brings out a short wavelength and reveals the presence of magnetic lineaments. For gravity anomalies and vertical magnetized bodies, the tilt derivative is positive over the source and negative outside it. Moreover, the merit of the TDR filter is that the zero-value contour line is located over or close to causative source boundaries. Accordingly, it can be used as an edge detector tool to outline the edge source bodies (e.g., contacts or faults).

The SPI method uses the local wavenumber from an analytical signal to calculate the depth of magnetic rocks. The SPI function is a quick, easy, and powerful method for calculating the depth of magnetic sources. SPI has the advantage of producing a more complete set of coherent solution points and it is easier to use. The resulting images of SPI method can be easily interpreted by someone who is an expert in local geology (Thurston and Smith 1997). The SPI depth can be estimated from the reciprocal local wavenumber as follows:

$$D = \frac{1}{K_{max}} = \frac{1}{\left(\sqrt{\left(\frac{\partial \text{Tilt}}{\partial x}\right)^2 + \left(\frac{\partial \text{Tilt}}{\partial y}\right)^2}\right)_{max}}, \tag{9}$$

where K is maximum value of the local wave number over a step source.

A 2D inverse modelling was carried out along two selected profiles using the GM-SYS program depending on the methods of Talwani et al. (1959) and Talwani and Heirtzler (1964). The first profile coded ($A-A'$) runs in the NE–SW direction, while the second coded ($B-B'$) runs in the NW–SE direction with a total length of 55 km and 68 km, respectively (Fig. 8). The results obtained from SPI were used to control the depth to the basement surface along the selected profiles. The assumed magnetic susceptibilities of the underlying basement rocks are taken to range from 0.0038 to 0.007 in c.g.s unit and a zero value for the overlain sedimentary cover. To create the model, parameters of the model such as magnetic susceptibility and depth were adjusted manually until the best matching between the observed and the calculated anomaly was obtained.

Results and discussion

The RTP map (Fig. 3b) in comparison with the TIM map (Fig. 3a) shows that the reduction process shifts the magnetic anomalies northward due to the elimination of the inclination and declination of the anomalies. The position and shape of the obtained magnetic anomalies are then related to their subsurface source bodies in the study area. The RTP map shows magnetic field intensity values between 42,045 nT as a minimum and 42,405 nT as a maximum. Qualitatively, a caution inspection of the RTP map

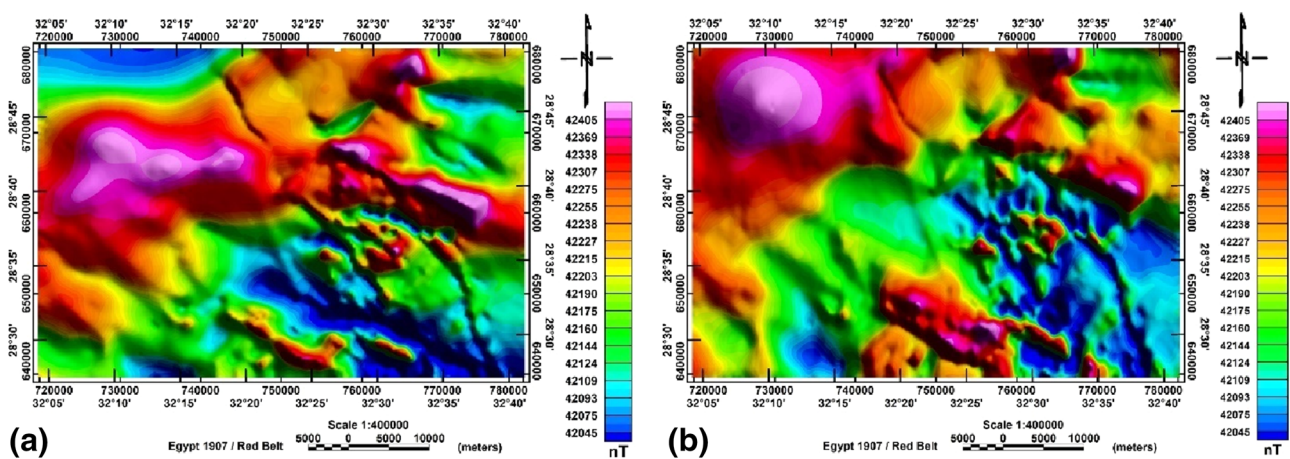


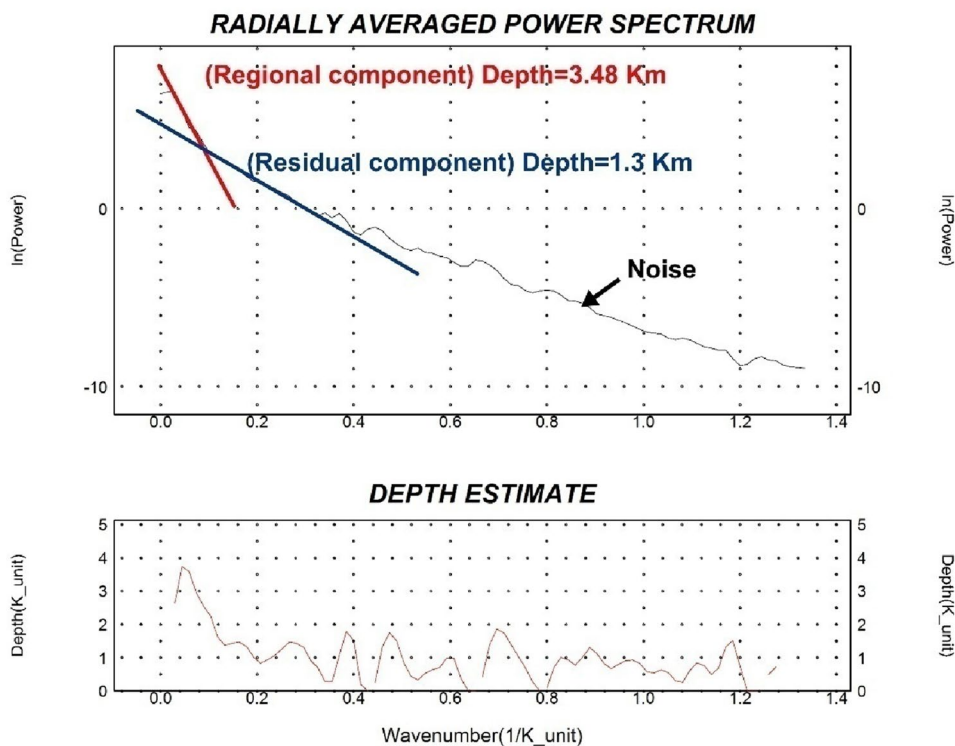
Fig. 3 (a) Colour shaded TIM map of study area (b) Colour shaded RTP map of study area

(Fig. 3b) reveals that the investigated area is characterized by the presence of a group of many magnetic anomalies of varying wavelengths, amplitudes, shapes, sizes, and magnitudes. This variation of magnetic field intensity reflects the variation of the causative bodies in depths or compositions. Accordingly, the study area can be divided into three zones with crucial magnetic characteristics. The first zone which occupies the southeastern part is characterized by low magnetic intensity values (the blue colour) that may be attributed to the presence of low magnetic susceptibility source bodies. Within this zone, there are clear spots of high magnetic intensity immersed in the surrounding low magnetic anomalies which can be interpreted as the presence of a magnetic source body with high magnetic susceptibility. In this zone, a very well correlation was achieved between the magnetic anomalies and their responsible causative bodies, where the surface geologic map (Fig. 2) elucidates the presence of exposed granitic rocks dominating this zone. The magnetic susceptibility of a rock depends on its magnetic content. Consequently, acidic igneous rocks are characterized by low susceptibilities, whereas the more basic rocks emanate higher susceptibility values (Milsom 2003). The second zone (green colour) is located in the central and the northeastern parts of the study area and is characterized by an intermediate magnetic response. Furthermore, the third zone (purple colour) is characterized by the presence of circular and elongated high magnetic intensity anomalies located in the northwestern, central southern and northeastern regions. The high magnetic response within the third

zone suggests the presence of basic or ultrabasic basement intrusions. The magnetic anomalies seem to be structurally controlled where most of them are oriented in NW–SE to NNE–SSW directions and the others are oriented in NE–SW and N–S directions. As the whole variation of crustal structure can be reflected by the disproportion of magnetic field intensity (Airo and Wennerström 2010), the spectrum curve (Fig. 4) was used to separate and define the shallow and the deep source bodies. Using a 0.08 cycle/km cut-off wavenumber depending on the slope changes of the power spectrum curve, the filtered regional and residual magnetic maps (Fig. 5) were obtained.

The regional magnetic anomaly map (Fig. 5a) displays the deep-seated causative sources with magnetic intensity varying from 42,075 to 42,400 nT. The high magnetic anomalies occupied the northwest, northeast and southern parts of the mapped area. On the other hand, the low magnetic anomalies dominated the central and the eastern parts. Most of the regional anomalies are oriented in the NW–SE direction (Gulf of Suez trend) as well as the presence of an E–W trend in the northwestern part of the area. Comparing the regional map (Fig. 5a) with the RTP map (Fig. 3b) reveals that there is a great similarity between them in the central and the western portions, thus indicating that the anomalies of the RTP map in these parts have regional roots. The residual magnetic anomaly map (Fig. 5b) is characterized by high frequencies, short wavelengths and small size magnetic anomalies which distinguish the near-surface structures in the study area. Examination of this map reveals that the study area

Fig. 4 Radial average power spectrum curve of RTP data manifesting the regional and residual components and their corresponding average depth



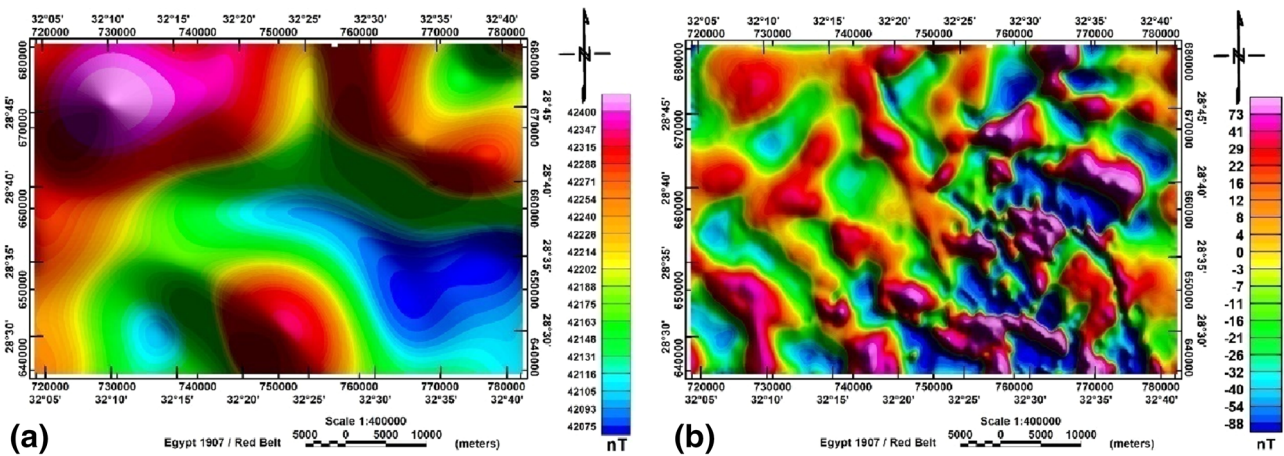


Fig. 5 (a) Colour shaded low pass filter magnetic map (regional) (b) Colour shaded high pass filter magnetic map (residual)

is characterized by the presence of numerous positive and negative small circular, oval, elongated and irregular-shaped magnetic anomalies, trending mainly in the NW–SE with a minor trace of NE–SW, N–S, and E–W directions. A high gradient between the alternative low and high anomalies is noticeable in the southeastern and the northeastern parts. Therefore, these features suggest the presence of faults and/or contacts located at shallow depths in this part more than in the rest of the area.

The HGM map (Fig. 6a) produces maxima ridges over the edges of contacts or faults. The most predominant trends traced from the HGM map (Fig. 6a) are the NW–SE, NNW–SSE and NE–SW trends and a minor trace of the N–S direction as shown from the azimuth frequency diagram (Fig. 6b). On the other hand, the AS map (Fig. 6c) exhibits maxima of anomalies located at the centre of the causative bodies. Given the azimuth frequency diagram (Fig. 6d), we can notice that the extracted lineaments from AS map trend at the NW–SE, NNW–SSE and NE–SW directions. The similarity in the lineaments pattern of the AS and HGM maps increases the result's reliability.

A glance on the geological map (Fig. 2) shows the presence of intrusions such as sills and dikes. The ED method (Thompson 1982; Reid et al. 1990) is used in this work for locating the source boundaries and their corresponding depths. In this manner, two ED solution maps were created for SI equal to 0.5 and 1 to analyse the locations and depths of faults and dykes, respectively (Fig. 7). ED solutions for SI=0.5 shows linear clustering solutions trending in the NW–SE and NE–SW directions (Fig. 7a). The same can be said in the ED map solution for SI=1 (Fig. 7b). Therefore, the coincidence of the spatial distribution of ED solutions of both dykes and faults leads to the conclusion that most of the intrusive rocks are controlled by the existing faults. The calculated depth solutions for the magnetic sources like faults and dykes vary between less than 500 to 1500 m (Fig. 7).

The extracted lineaments map from the CET grid analysis techniques (Fig. 8a) shows that the orientations of these lineaments are in the WNW–ENE, NW–SE, N–S and NE–SW directions, as shown in the plotted rose diagram (Fig. 8b). The TDR map (Fig. 9) can be used easily to outline the geological structures like faults through tracking the zero value of the contour line which refer to the location of abrupt changes in magnetic susceptibility values. The zero-contour lines in the TDR map (Fig. 9) are represented by black colour. The main structural trends deduced from the TDR map are oriented in the NW–SE and NE–SW directions. The appearance and the orientation of shallow TDR magnetic anomalies are consistent with that previously shown in the AS and HGM maps (Fig. 6a, c). A correlation between different EDT results was made by plotting the solutions of ED for SI 0.5 (Fig. 7a) and the extracted lineaments map from the CET grid analysis (Fig. 8a) on the TDR map (Fig. 9), thus, to ensure the reliability degree of EDT results. Figure 9 shows that the depth solutions of ED for SI equal to 0.5 is congruous with the location of the source edges along with the zero-contour line of the TDR map. On the other hand, the CET results (white lines) are superimposed along with the locations of both ED solutions of the fault and zero-contour line of the TDR map and a good correlation between them was achieved, which increases the reliability of the results as the ED, TDR, and CET grid analysis represent good edge detector tools for mapping subsurface structures.

From the previous discussion of EDT, it is clear that the NW–SE, NNW–SSE and NE–SW represents the main structural trends affecting the study area. The NW–SE and NNW–SSE trends are related to the Gulf of Suez and the Red Sea rifting system trend, which formed during the early Tertiary. The Mesozoic–Cenozoic structural deformation of Egypt is a result of the movement of the African Plate and the surrounding plates resulted in NE–SW, NW–SE, and NNW–SSE directions (Hamimi et al. 2020). The overall

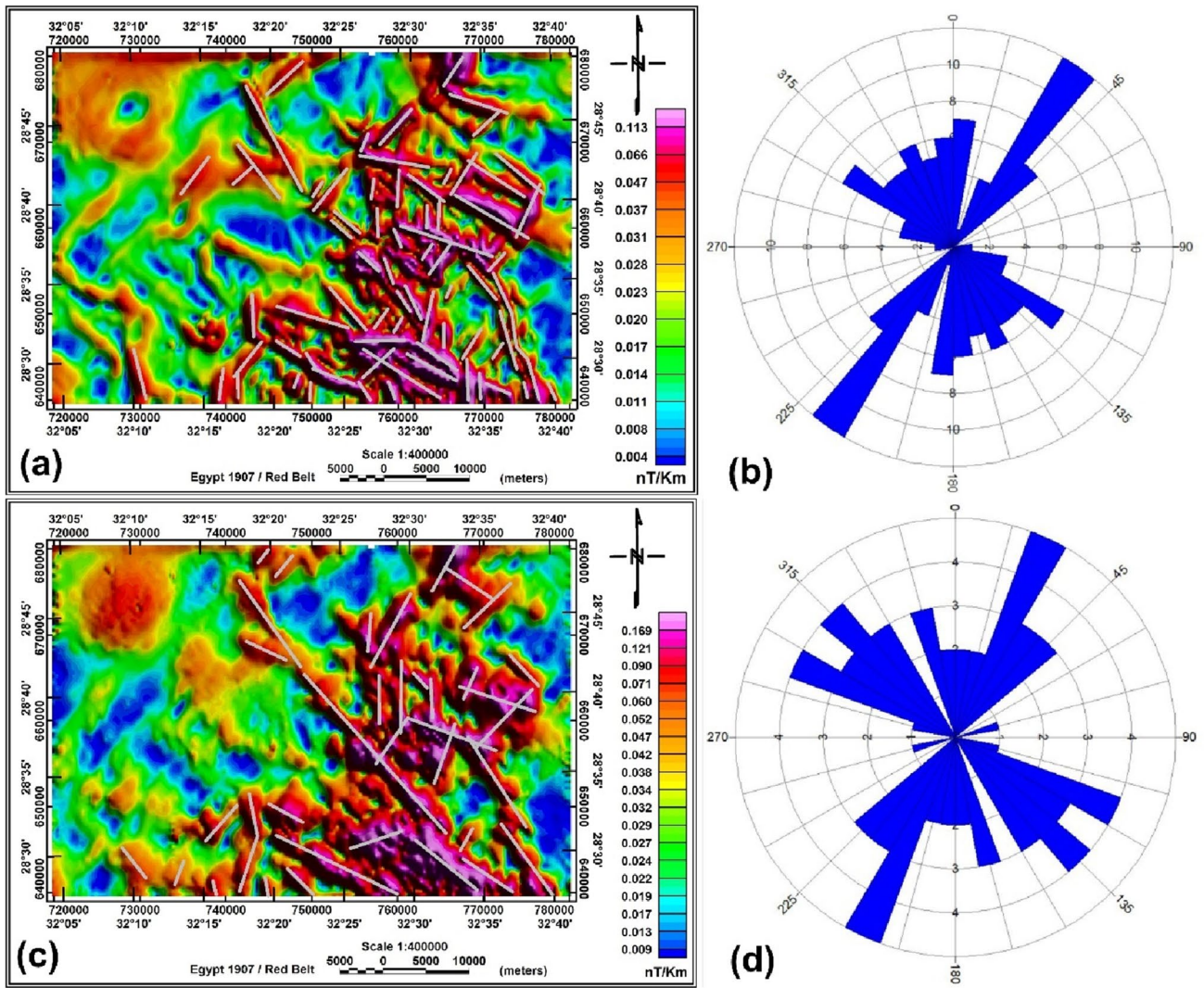


Fig. 6 (a) Colour shaded HGM map of the study area (b) Rose diagram showing trends orientation as extracted from HGM map (c) Colour shaded AS map of the study area (d) Rose diagram showing trends orientation as extracted from AS map

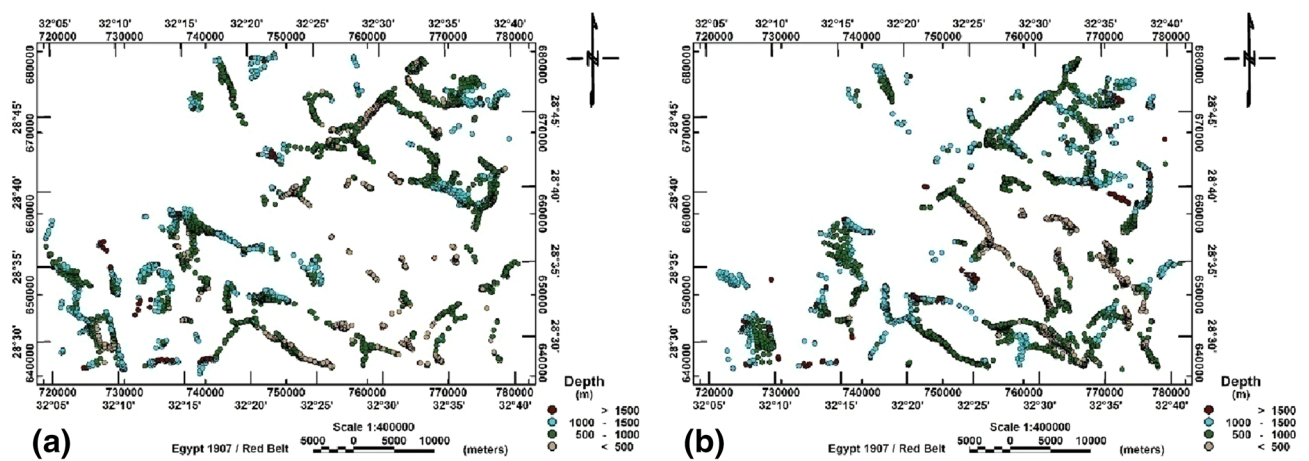


Fig. 7 (a) ED solutions map for SI (0.5) define location and depth of faults (b) ED solutions map for SI (1) define location and depth of dykes

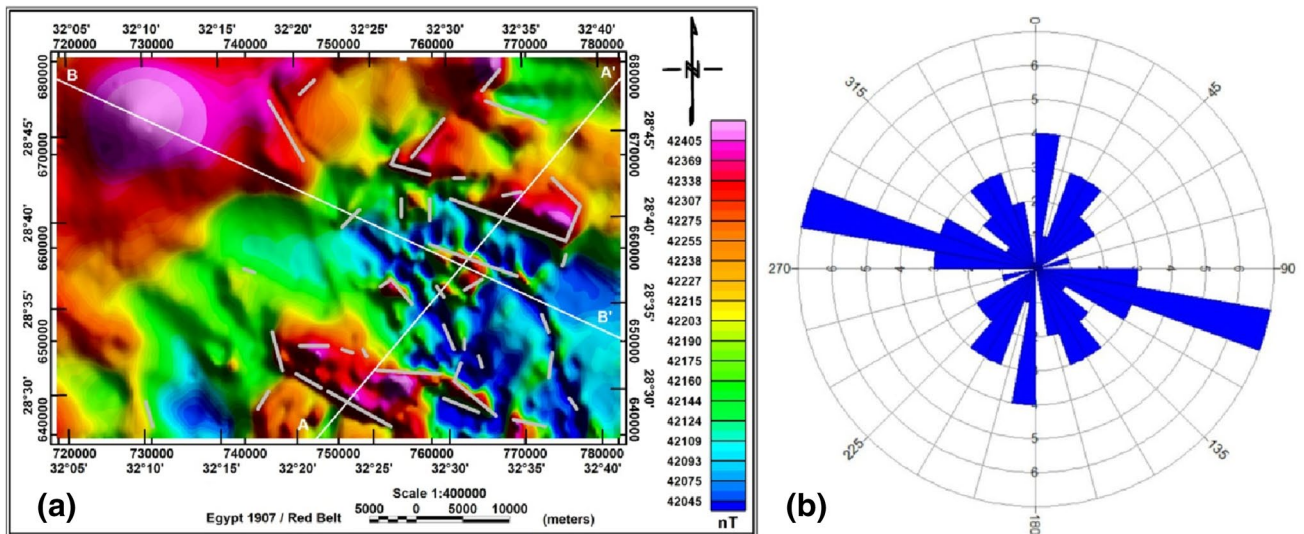
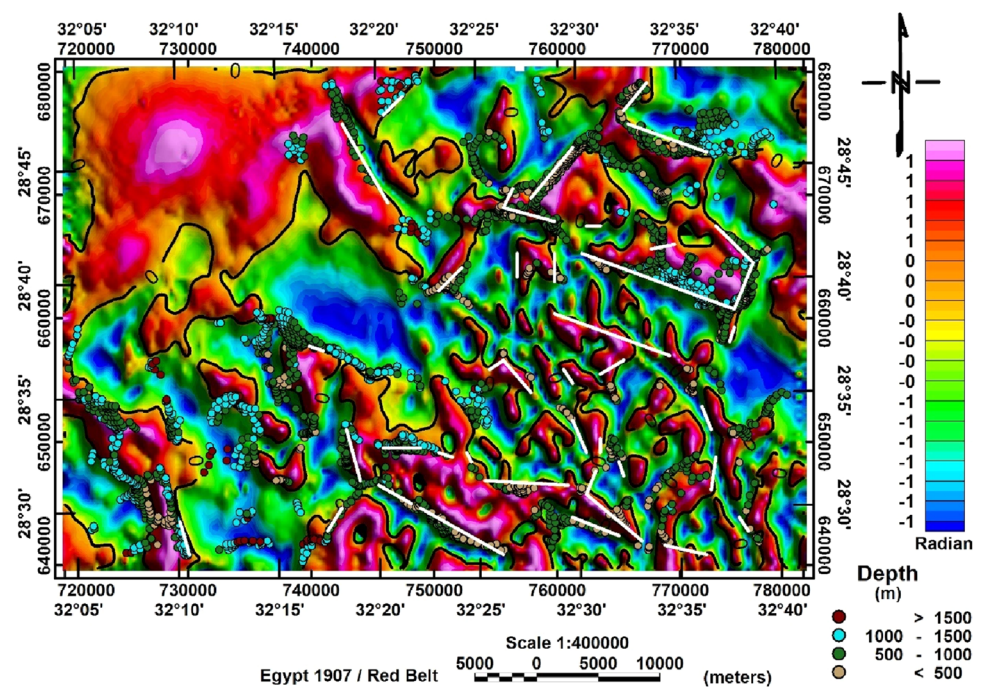


Fig. 8 Extracted lineaments from CET grid analysis superimposed on RTP map (gray lines) and the location of two2D profiles taken along the RTP map (white lines)

Fig. 9 ED solutions depth for SI 0.5 and the extracted lineaments of the CET grid analysis (white lines) plotted on the shaded colour TDR map matched with zero-contour line of TDR map



EDT results indicate that the study area is structurally controlled, and the extracted lineaments could be favourable structures like faults, fractures, contacts for mineralization existing, since (Megwara and Udensi 2014) had earlier obvious that, the lineaments density are related to mineralization.

The average depths of the magnetic sources have been estimated based on the analysis of the power spectrum curve (Fig. 4). From the power spectrum curve, there are two linear segments with different slopes. The first segment (red line) represents the regional components of magnetic

anomaly, while the second (blue line) represents the residual components of magnetic anomaly. Then, the depth to the top of the causative bodies can be estimated by dividing the obtained slope by the factor (4π) (Spector and Grant 1970). Accordingly, the estimated average depths for the deep and shallow magnetic components are about 3.48 km and 1.3 km, respectively. Moreover, the AS and SPI depth maps (Fig. 10) provided a more detailed picture of the distributions of basement depths over the study area. The AS map (Fig. 10a) shows that the depth of the basement varies

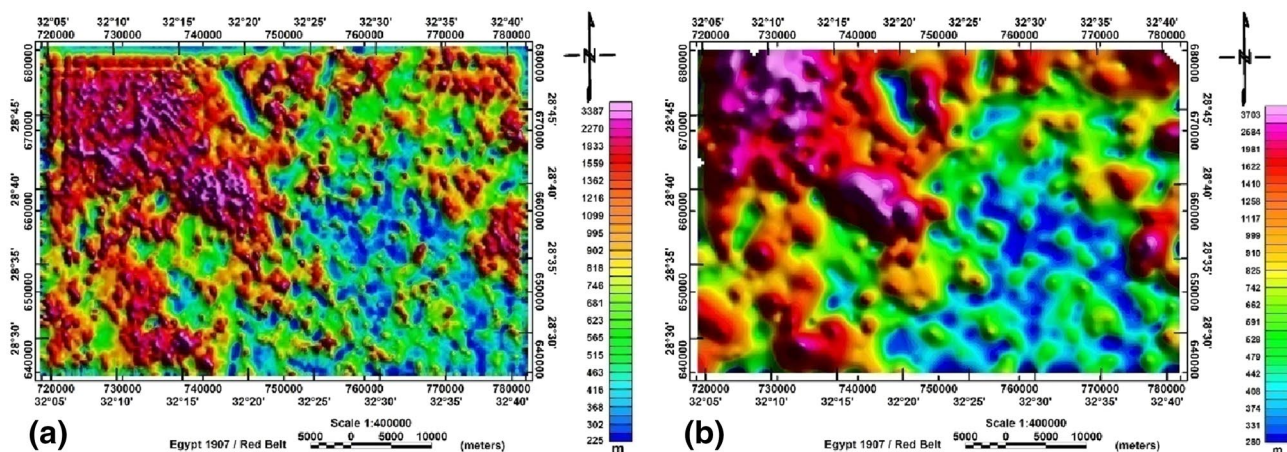


Fig. 10 (a) AS depth map of El Galala El Qibliya plateau area (b) SPI depth map of El Galala El Qibliya plateau area

between 225 and 3387 m. The SPI map (Fig. 10b) reflects a range of depths between 280 and 3703 m below the surface. These results are more or less similar, thus reinforcing the obtained estimated depths. On the other hand, both of them reflect that the shallower depth to the basement is located in the southeastern part of the study area, while the deepest part exists in the northwestern part beneath the plateau of El Galala El Qibliya.

Two magnetic profiles were taken along the RTP map (Fig. 8) the first is passing from the SW–NE, while the second is passing from the NW–SE direction. The constructed two 2D magnetic models (Fig. 11) manifest a good illustration of the depth and susceptibility of the basement blocks. The first profile denoted as (A–A′) was modelled using three polygons with magnetic susceptibility varies between 0.0038 and 0.005 cgs unit (Fig. 11a). This model shows that the basement surface in general is located at a shallow depth ranging from 50 to 500 m along the most part of the profiles except for the southwestern part exhibits a maximum depth of 900 m. The second model coded as (B–B′) (Fig. 11b) consists of three basement blocks with magnetic susceptibility ranges between 0.0038 and 0.007 which reflects the variations in the composition of these basement blocks. The basement surface is characterized by an irregular surface with a horst-graben configuration of basement morphology which is controlled by block faulting that may affect the overlying sedimentary cover and that may enhance the migration and entrapment of hydrocarbon in sedimentary succession. At the distance of 44 km from the starting point of the profile, the basement surface is exposed at the surface then the depth increased gradually towards the NW direction to reach its maximum of 3500 m. At the southeastern part of the modelled profile, the maximum depth of the basement surface recorded a depth of 2500 m below the surface. The modelled profiles in general, show that the study area consists

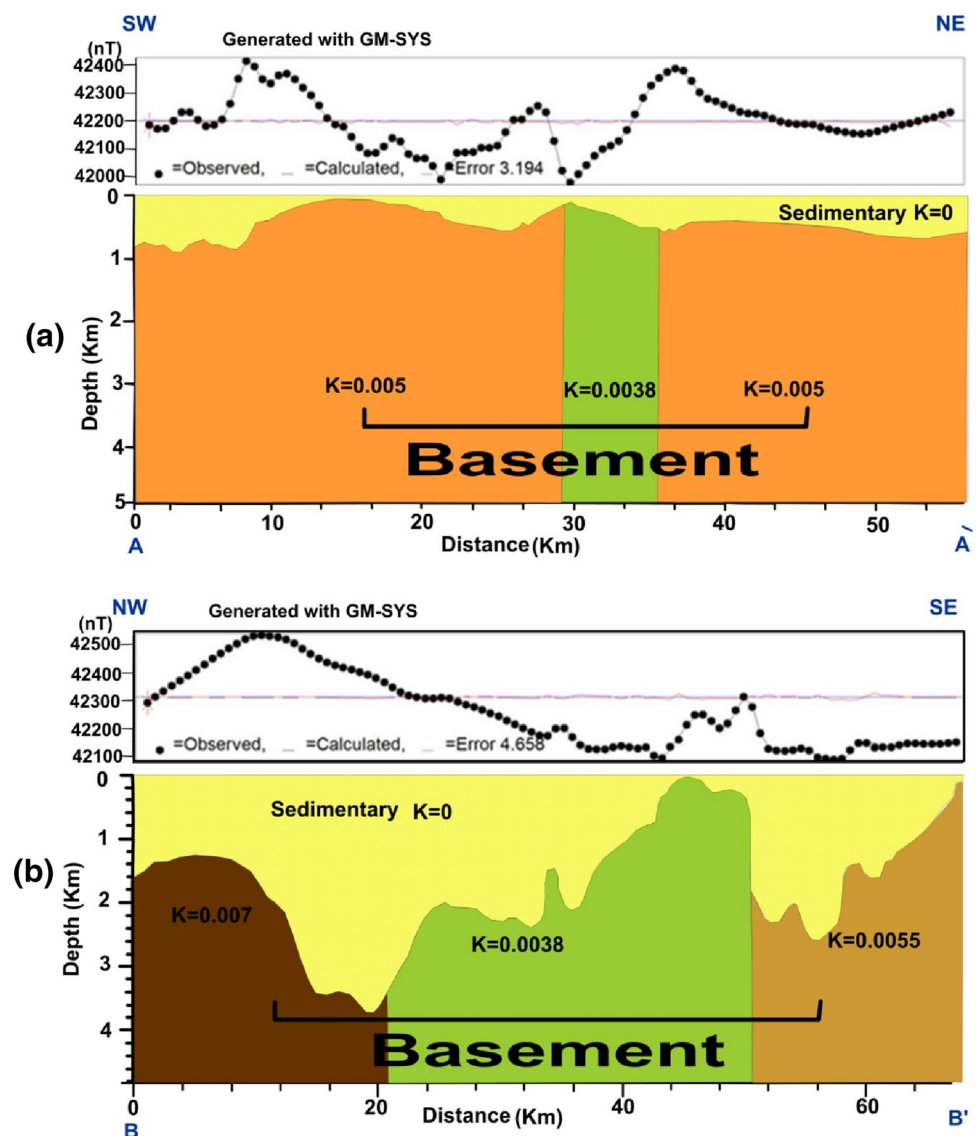
of basement blocks with various components as illustrated by the variations of magnetic susceptibility of the modelled basement blocks (Fig. 11). The highest recorded value of magnetic susceptibility is existing at the northwestern part of the modelled profile (B–B′) (Fig. 11b) which located beneath El Galala El Qibliya plateau and that may be due to the presence of a basic rock underlain the sedimentary succession. That is why a high magnetic intensity value of the RTP map (Fig. 3a) appears at this part of the study area. The higher magnetic intensity values are associated with higher magnetic susceptibility values due to the abundance of ferromagnetism minerals occurring in the basic or ultrabasic rocks (Hunt et al. 1995).

The overall results obtained from the different depth estimation methods prove that the sedimentary thickness in some parts of the study area, such as the northwestern part, reaches more than 3500 m. On the other hand, the lowest thickness of sediments exists on the southeastern side of the area where some exposures of rock units appear at the surface. Finally, the analysis of the aeromagnetic data at El Galala El Qibliya plateau contributes to mapping subsurface structures, determining the basement depth, and sedimentary cover thickness.

Conclusions

The interpretation of the available aeromagnetic data contributes to delineate the basement configurations and the structures set up in the study area. The obtained results show two main trends affecting the area: the first is related to the Gulf of Suez trend with NW–SE direction, and the second belongs to the Gulf of Aqaba trend with an orientation of NE–SW. The basement architecture affected by these trends appears as alternative horsts and grabens-like features

Fig. 11 (a) 2D model of profile (A–A') (b) 2D model of profile (B–B')



resulting in a variable thickness of the overlain sedimentary succession across the study area. The basement depth varies between 225 to 3700 m as deduced from the SPI and AS depth estimation methods, with averages of 3489 m and 1300 m for the deep and shallow magnetic sources, respectively, as inferred from the analysis of the spectrum curve.

The EDT results shows that, the southeastern and the northeastern part of the area characterized by high lineaments density than the other parts that suggest a more abundance of faults, fractures, and lithological contacts which may be possible locales for mineral resources. The deepest part of the basement surface exists beneath El Galala plateau on the northwestern side of the area, where it gives a maximum accumulation of sedimentary thickness that exceed 3400 m. The sedimentary cover thickness in the study area attains about 3500 m and this is promising for oil accumulation in such area, since Wright

et al. (1985) claims that a minimum of 2300 m sedimentary rock thickness is required for hydrocarbon generation from organic remains..

This work adds more information about the basement morphology and structure pattern at El Galala El Qibliya plateau area as a reconnaissance study for hydrocarbon and mineral prospecting. The Egyptian government should support further studies at El Galala El Qibliya plateau area for exploring hydrocarbon and mineral resources.

Acknowledgements The authors are so grateful to the reviewers of the Modeling Earth Systems and Environment journal for their beneficial reviewing.

Declarations

Conflict of interest The authors declare that there are no known competing interests regarding this work.

References

- Abdelazeem M, Fathy MS, Khalifa MM (2019) Integrating magnetic and stratigraphic data to delineate the subsurface features in and around new Galala City, Northern Galala Plateau, Egypt. *NRIAG J Astron Geophys* 8:131–143. <https://doi.org/10.1080/20909977.2019.1627634>
- Abdel-Gawad M (1970) A discussion on the structure and evolution of the Red Sea and the nature of the Red Sea, Gulf of Aden and Ethiopia rift junction—The Gulf of Suez: a brief review of stratigraphy and structure. *Philos Trans R Soc London Ser a, Math Phys Sci* 267:41–48. <https://doi.org/10.1098/rsta.1970.0022>
- Aero service (1984) Final report on airborne magnetic/radiation survey in Eastern Desert, Egypt. Work Completed for the Egyptian General Petroleum Corporation (EGPC). Six volumes, Aero Service, Houston, Texas, USA.
- Airo M-L, Wennerström M (2010) Application of regional aeromagnetic data in targeting detailed fracture zones. *J Appl Geophys* 71:62–70. <https://doi.org/10.1016/j.jappgeo.2010.03.003>
- Al-Saud MM (2014) The role of aeromagnetic data analysis (using 3D Euler deconvolution) in delineating active subsurface structures in the west central Arabian shield and the central Red Sea, Saudi Arabia. *Arab J Geosci* 7:4361–4376. <https://doi.org/10.1007/s12517-013-1068-1>
- Anyadiegwu CF, Ijeh BI, Ohaegbuchi HE (2017) 3D modelling of subsurface features in parts of the Lower Benue Trough, south-eastern Nigeria, with high resolution aeromagnetic data. *Model Earth Syst Environ* 3:943–962. <https://doi.org/10.1007/s40808-017-0344-6>
- Araffa SAS, Alrefae HA, Nagy M (2020) Potential of groundwater occurrence using geoelectrical and magnetic data: A case study from south Wadi Hagul area, the northern part of the Eastern Desert, Egypt. *J Afr Earth Sci* 172:103970. <https://doi.org/10.1016/j.jafrearsci.2020.103970>
- Azab AA (2020) Integration of seismic and potential field data analysis for deducing the source structures in Ras Amer oil field, Gulf of Suez, Egypt. *Arab J Geosci* 13:190. <https://doi.org/10.1007/s12517-020-5082-9>
- Baranov V, Naudy H (1964) Numerical calculation of the formula of reduction to the magnetic pole. *Geophysics* 29:67–79
- Basantaray AK, Mandal A (2022) Interpretation of gravity–magnetic anomalies to delineate subsurface configuration beneath east geothermal province along the Mahanadi rift basin: a case study of non-volcanic hot springs. *Geotherm Energy* 10:6. <https://doi.org/10.1186/s40517-022-00216-4>
- Conoco Inc (1987) Geological map of Egypt 1:500 000, The Egyptian General Petroleum Corporation
- Conoco Inc (1989) Stratigraphic lexicon and explanatory notes to the geological map of Egypt, Scale 1:500,000. conoco Inc., Cairo, Egypt
- Cordell L, Grauch VJS (1985) Mapping basement magnetization zones from aeromagnetic data in the San Juan Basin, New Mexico. In: *The Utility of regional gravity and magnetic anomaly maps. Society of Exploration Geophysicists*, pp 181–197
- Dentith M, Mudge ST (2014) *Geophysics for the mineral exploration geoscientist*. Cambridge University Press, Cambridge
- El-Sadek MA (2009) Subsurface structural mapping of the area lying between Gabal Elgalala Elqibliya and Elgalala Elbahariya, Northern Eastern Desert, Egypt. *J Geophys Eng* 6:111–119. <https://doi.org/10.1088/1742-2132/6/2/002>
- Erbek E (2021) An investigation on the structures and the basement depth estimation in the western Anatolia, Turkey using aeromagnetic data. *Geosci J* 25:891–902. <https://doi.org/10.1007/s12303-021-0001-y>
- Eweis AM, Toni M, Basheer AA (2022) Depicting the main structural affected trends by operating aeromagnetic survey in the western part of Koraimat-Alzafarana road and surround area, Eastern Desert, Egypt. *Model Earth Syst Environ* 8:2803–2816. <https://doi.org/10.1007/s40808-021-01265-7>
- Ghazala HH, Ibraheem IM, Haggag M, Lamees M (2018) An integrated approach to evaluate the possibility of urban development around Sohag Governorate, Egypt, using potential field data. *Arab J Geosci* 11:194. <https://doi.org/10.1007/s12517-018-3535-1>
- Hamath M, Ja M, Lo K et al (2020) Mapping mafic dyke swarms, structural features, and hydrothermal alteration zones in Atar, Ahmeyim and Chami areas (Reguibat Shield, Northern Mauritania) using high-resolution aeromagnetic and gamma-ray spectrometry. *J Afr Earth Sci* 163:1–13. <https://doi.org/10.1016/j.jafrearsci.2019.103749>
- Hamimi Z, El-Barkooky A, Martínez Frías J et al (eds) (2020) *The geology of Egypt*. Springer International Publishing, Cham
- Hinze WJ, Von Ferse RRB, Saad AH (2013) *Gravity and magnetic exploration principles, practices, and applications*. Cambridge University Press, Cambridge
- Holden E, Wong JC, Kovessi P et al (2012) Identifying structural complexity in aeromagnetic data: an image analysis approach to greenfields gold exploration. *Ore Geol Rev* 46:47–59. <https://doi.org/10.1016/j.oregeorev.2011.11.002>
- Hunt CP, Moskowitz BM, Banerjee SK (1995) Magnetic properties of rocks and minerals. *Rock Phys Phase Relat A Handb Phys Constants* 3:189–204
- Ibraheem IM, Elawadi EA, El-Qady GM (2018) Structural interpretation of aeromagnetic data for the Wadi El Natrun area, northwestern desert, Egypt. *J Afr Earth Sci* 139:14–25. <https://doi.org/10.1016/j.jafrearsci.2017.11.036>
- Ismail AA, Boukhry M (2001) Campanian larger foraminifera of Gebel Thelmet formation (Stratotype), Southern Galala, Eastern Desert, Egypt. *Rev Paléobiol* 20:77–90
- Keheila E (2000) Lower Eocene facies, environments and evolution of sedimentary basins in southern Galala, Egypt: evidence for global coastal onlap and tectonics. In: *2nd International Conference on the Basic Sciences and Technology, Assiut, Egypt*. pp 75–104
- Kuss J (1986) Facies development of upper cretaceous—lower tertiary sediments from the monastery of St. Anthony/Eastern Desert, Egypt. *Facies* 15:177–193
- Kuss J, Leppig U (1989) The early Tertiary (middle-late Paleocene) limestones from the western Gulf of Suez, Egypt. *Neues Jahrb Für Geol Und Paläontologie* 177:289–332
- Kuss J, Scheibner C, Gietl R (2000) Carbonate platform to basin transition along an upper cretaceous to lower tertiary Syrian arc uplift, Galala Plateaus, Eastern desert of Egypt. *GeoArabia* 5:405–424. <https://doi.org/10.2113/geoarabia0503405>
- Megwara JU, Udensi EE (2014) Structural analysis using aeromagnetic data: case study of parts of southern Bida Basin, Nigeria and the surrounding basement rocks. *Earth Sci Res*. <https://doi.org/10.5539/esr.v3n2p27>
- Mekkawi MM, Abd-El-Nabi SH, Farag KS, Abd Elhamid MY (2022) Geothermal resources prospecting using magnetotelluric and magnetic methods at Al Ain AlSukhuna-Al Galala Albahariya area, Gulf of Suez, Egypt. *J Afr Earth Sci* 190:104522. <https://doi.org/10.1016/j.jafrearsci.2022.104522>
- Miller HG, Singh V (1994) Potential field tilt—a new concept for location of potential field sources. *J Appl Geophys* 32:213–217. [https://doi.org/10.1016/0926-9851\(94\)90022-1](https://doi.org/10.1016/0926-9851(94)90022-1)
- Milsom J (2003) *Field geophysics_The geological field guide series, 3rd edn*. Wiley, New York
- Mohamed HS, Zaher MA (2020) Subsurface structural features of the basement complex and geothermal resources using aeromagnetic data in the Bahariya oasis, western desert, Egypt. *Pure Appl Geophys* 177:2791–2802. <https://doi.org/10.1007/s00024-019-02369-z>

- Moustafa AR, Khalil MH (1995) Superposed deformation in the northern Suez rift, Egypt: relevance to hydrocarbons exploration. *J Pet Geol* 18:245–266. <https://doi.org/10.1111/j.1747-5457.1995.tb00905.x>
- Nabighian MN (1972) The analytic signal of two-dimensional magnetic bodies with polygonal cross-section: its properties and use for automated anomaly interpretation. *Geophysics* 37:507–517. <https://doi.org/10.1190/1.1440276>
- Nathan D, Aitken A, Holden EJ, Wong J (2020) Imaging sedimentary basins from high-resolution aeromagnetics and texture analysis. *Comput Geosci* 136:104396. <https://doi.org/10.1016/j.cageo.2019.104396>
- Oguama BE, Okeke FN, Obiora DN (2021) Mapping of subsurface structural features in some parts of Anambra Basin, Nigeria, using aeromagnetic data. *Model Earth Syst Environ* 7:1623–1637. <https://doi.org/10.1007/s40808-020-00894-8>
- Okoro ME, Onuoha MK, Opara AI et al (2022) Structural styles and basement architecture of the Dahomey basin southwestern Nigeria from aeromagnetic data. *Arab J Geosci* 15:456. <https://doi.org/10.1007/s12517-022-09703-1>
- Osinowo OO, Alumona K, Olayinka AI (2020) Analyses of high resolution aeromagnetic data for structural and porphyry mineral deposit mapping of the nigerian younger granite ring complexes, North-Central Nigeria. *J Afr Earth Sci* 162:103705. <https://doi.org/10.1016/j.jafrearsci.2019.103705>
- Phillips JD (2002) Processing and interpretation of aeromagnetic data for the santa cruz basin--patagonia mountains area, South-central Arizona. US Department of the Interior, US Geological Survey Washington, DC, USA
- Pohl WL (2011) *Economic geology, principles and practice*. Wiley-Blackwell, New York
- Ramotoroko C, Shemang E, Lushetile B, Sitali M (2021) Curie point depth analysis of aeromagnetic data of Kasane region in northwest Botswana and surrounding regions for geothermal investigation of Kasane Hot Spring. *J Afr Earth Sci* 180:104214. <https://doi.org/10.1016/j.jafrearsci.2021.104214>
- Reid AB, Allsop JM, Granser H et al (1990) Magnetic interpretation in three dimensions using Euler deconvolution. *Geophysics* 55:80–91
- Reynolds JM (2011) *An introduction to applied and environmental geophysics*, 2nd edn. Wiley-Blackwell, New York
- Roest WR, Verhoef J, Pilkington M (1992) Magnetic interpretation using the 3-D analytic signal. *Geophysics* 57:116–125. <https://doi.org/10.1190/1.1443174>
- Saada SA (2016) Edge detection and depth estimation of Galala El Bahariya Plateau, Eastern Desert-Egypt, from aeromagnetic data. *Geomech Geophys Geo-Energy Geo-Resour* 2:25–41. <https://doi.org/10.1007/s40948-015-0019-6>
- Scheibner C, Marzouk A, Kuss J (2001) Shelf architectures of an isolated Late Cretaceous carbonate platform margin, Galala Mountains (Eastern Desert, Egypt). *Sediment Geol* 145:23–43. [https://doi.org/10.1016/S0037-0738\(01\)00114-2](https://doi.org/10.1016/S0037-0738(01)00114-2)
- Spector A, Grant FS (1970) Statistical models for interpreting aeromagnetic data. *Geophysics* 35:293–302
- Talwani M, Heirtzler JR (1964) Computation of magnetic anomalies caused by two-dimensional bodies of arbitrary shape. *Comput Miner Ind* 1:464–480
- Talwani M, Worzel JL, Landisman M (1959) Rapid gravity computations for two-dimensional bodies with application to the Mendocino submarine fracture zone. *J Geophys Res* 64:49–59. <https://doi.org/10.1029/JZ064i001p00049>
- Thompson DT (1982) EULDPH: a new technique for making computer-assisted depth estimates from magnetic data. *Geophysics* 47:31–37
- Thurston JB, Smith RS (1997) Automatic conversion of magnetic data to depth, dip, and susceptibility contrast using the SPI (TM) method. *Geophysics* 62:807–813. <https://doi.org/10.1190/1.1444190>
- Tsokas GN, Papazachos CB (1992) Two-dimensional inversion filters in magnetic prospecting: application to the exploration for buried antiquities. *Geophysics* 57:1004–1013. <https://doi.org/10.1190/1.1443311>
- Wright JB, Hastings DA, Jones WB, Williams HR (1985) *Geology and mineral resources of West Africa*. Springer
- Younes AI, McClay K (2002) Development of accommodation zones in the Gulf of Suez-Red Sea rift, Egypt. *Am Assoc Pet Geol Bull* 86:1003–1026. <https://doi.org/10.1306/61EEDC10-173E-11D7-8645000102C1865D>

Publisher's Note Springer Nature remains neutral with regard to jurisdictional claims in published maps and institutional affiliations.

Springer Nature or its licensor (e.g. a society or other partner) holds exclusive rights to this article under a publishing agreement with the author(s) or other rightsholder(s); author self-archiving of the accepted manuscript version of this article is solely governed by the terms of such publishing agreement and applicable law.